

Comprehensive Study of Properties of a Endohedrally Confined Ca Atom using Relativistic Many-body Methods

S. Bharti¹, L. Sharma¹, B. K. Sahoo², P. Malkar¹ and R. Srivastava¹

¹*Department of Physics, Indian Institute of Technology Roorkee, Roorkee 247667, India*

²*Atomic, Molecular and Optical Physics Division,*

Physical Research Laboratory, Navrangpura, Ahmedabad 380009, India

(Dated: November 16, 2018)

We have carried out theoretical investigations of electron correlation effects on the atomic properties of the Ca atom trapped inside an attractive spherically symmetric potential well of an endohedral fullerene C₆₀ cluster. Relativistic coupled-cluster (RCC) theory has been employed to obtain electron correlation energy, ionization potential and dipole polarizability of this atom. We have also performed calculations using the Dirac-Hartree-Fock (DF), relativistic second-order many-body perturbation theory (RMBPT(2) method) and relativistic random phase approximation (RRPA) to demonstrate propagation of the correlation effects in these properties. Our results are compared with the reported calculations employing multi-configuration Hartree-Fock (MCHF) method in Phys. Rev. A **87**, 013409 (2016). We found trends in correlation energy with respect to the potential depth are same, but magnitudes are very large in the relativistic calculations. We have also determined the differential and total cross-sections for elastic scattering of electrons from the free and confined Ca atoms using the electronic charge densities from the Dirac-Hartree core-potential (DFCP) and RCC methods to demonstrate role of potential depth in these properties.

PACS numbers:

I. INTRODUCTION

Studies related to confined atoms are important for a broad range of possible applications. The spatial entrapment of atoms or molecules is possible in nature as well as artificially; e.g., impurity atoms in mesoscopic scale semiconductor artificial structures, molecular zeolite sieves, fullerenes, quantum devices, etc. [1, 2]. The confinement of atoms lead to distinct and interesting changes in their electronic structures and other properties. Endohedral entrapment of an atom inside fullerene cage can be synthesized in laboratory owing to rapid developments in the modern technologies. These endohedral fullerenes unveil interesting physical and chemical properties that can be significantly different from the encapsulated atom or the fullerene itself. Although studies of confined endohedral atoms in any fullerene are interesting, but confined atoms particularly in the C₆₀ fullerene has drawn more attention these days. This is because C₆₀ can be assumed as a spherical ball with the confined atom at the center. Therefore, the energy levels of a confined atom can still be described using a spherical potential as for a free atom by suitably choosing an effective potential.

Using R-matrix method in the non-relativistic theory, Hasoğlu *et al.* [3] had calculated cross-sections for the photoionization process of a confined Ca atom and reported the influence of potential well depth on near threshold photoionization cross-sections. Following this work, Kumar *et al* [4] had investigated non-dipole effects in photoionization of outer 4s shell of the entrapped Ca atom in a spherical attractive well potential in the relativistic random phase approximation (RRPA). Recently, Hasoğlu *et al.* [5] have investigated electron correlation effects of endohedral confinement on the energy levels

of Be, Mg, and Ca atoms in the non-relativistic framework using multi-configuration Hartree-Fock (MCHF) method. Hasoğlu *et al.* have argued in their work about the possibility of confinement of Ca atom at the center of the C₆₀ shell, giving rise to a stable equilibrium. It is, therefore, imperative to understand energy levels of such an environment on the structure of a captured Ca atom more accurately by employing a powerful relativistic many-body method before carrying out experiment.

It is very challenging to get accurate results for the atomic properties of the Ca atom even when it is isolated from any external mediation owing to strong correlations between its two valence s electrons. For example, it has been found earlier that the lower-order relativistic perturbative theories underestimate the electric dipole polarizability (α_0) value of the Ca atom while RRPA overestimates it compared to the experimental value [6]. As mentioned above, only a few less powerful many-body methods are employed to account for electron correlation effects in the confined Ca atom. To guide future experiment on the confined Ca atom, it is necessary to study its spectroscopic properties by applying a more accurate theory. In this work, we have calculated many properties such as electron correlation energy, ionization potential (IP) and α_0 of the confined Ca atom in the endohedral fullerene C₆₀ cluster and show their variation with the attractive potential depth. These calculations are performed within the framework of the Dirac-Hartree-Fock (DF) method, relativistic second-order many-body perturbation theory (RMBPT(2) method), RRPA and relativistic coupled-cluster (RCC) theory. We employ the lower-order methods like DF and RMBPT(2) methods in order to find out role of electron correlations in the above properties by comparing results from these methods. The RCC theory is an all-order perturbative method

that obeys proper scaling with the number of electrons even when it is approximated in contrast to the truncated configuration interaction (CI) method or its variants like the MCHF method [7–9]. It also includes core-polarization effects to all-order as in RRPA along with other physical effects. To ascertain accuracies of the results, we first perform calculations of the aforementioned properties of the free Ca atom and compare them with their corresponding experimental values. We also compare our calculations of self-consistent field (SCF) energy and energies of the $4s$, $3p_{3/2}$, $3p_{1/2}$ and $3s$ orbitals at various depths of the confining annular potential well with the earlier reported results by Kumar *et al.* using the DF method [4].

Because of experimental feasibility to prepare confined atoms, the interest in electron elastic collision with entrapped atoms is increasing now-a-days [10–13]. However, there have been few theoretical studies reported in the context of elastic scattering of electrons from confined atom A@C₆₀. Dolmatov *et al.* have studied elastic collision of low energy electrons with A@C₆₀ and demonstrated the role of polarizability of an atom + C₆₀ [10] and that of atoms alone [11]. In fact, Dolmatov *et al.* have given a full account of the previous related works in Refs. [10, 11] on the same. However, these studies were carried out using non-relativistic Hartree-Fock theory and at low projectile electron energies. Here, we have performed calculations of the elastic collision cross-sections for the intermediate projectile electrons scattered from the endohedrally confined Ca atoms in the relativistic theory framework. Furthermore, we have used electron charge densities from the DF method, DF method with core-polarization (CP) potential (DFCP method) and RCC theory to show the differences in the results due to various approximations in the many-body methods. It to be noted that RCC theory includes CP potential to all-orders along with electron correlations due to non-CP type of interactions. In all these approaches, we take into account the quantum mechanical exchanges between the projectile and atomic electrons as well as polarizability of the atom as a function of potential depth. Since we focus only on the effect of confinement of Ca on electron scattering process, we have neglected the impact of polarizability of C₆₀ by the incident electron in these calculations. The results are reported for differential cross-sections (DCSs) and integrated cross-sections (ICSs). We compare our results for the free Ca atom with the available experimental data [14] and other reported calculations using the DFCP method [15] in order to gauge accuracies of the results for the confined atom.

II. METHODS FOR CALCULATIONS

A. Atomic properties

In the DF method, we obtain the mean-field wave function $|\Phi_0\rangle$ using the V^N potential of the $[3p^64s^2]$ configuration of the Ca atom. All the DF and DFCP results are obtained using this wave function and $\alpha_0 = 169 ea_0^3$ from experiment [16]. The exact wave function in the RCC theory is expressed using $|\Phi_0\rangle$ as the reference determinant as [17]

$$|\Psi_0\rangle = e^{\hat{T}}|\Phi_0\rangle, \quad (1)$$

where \hat{T} is known as the RCC excitation operator given by

$$\hat{T} = \sum_{k=1}^N \hat{T}_k = \sum_{\substack{a_1 < a_2 \dots < a_k \\ i_1 < i_2 \dots < i_k}} t_{i_1 i_2 \dots i_k}^{a_1 a_2 \dots a_k} a_1^+ i_1^- a_2^+ i_2^- \dots a_k^+ i_k^- \quad (2)$$

with + and – superscripts on the second quantization operators represent for creation and annihilation of electrons in the virtual (denoted by a) and occupied (denoted by i) orbitals, respectively, and t are the amplitudes in the excitation process in an N electron system. The RCC approaches considering up to T_N operators with $N = 2, 3, 4, \dots$, known as the RCC singles and doubles (RCCSD), RCC singles, doubles, and triples (RCCSDT), RCC singles, doubles, triples, and quadruples (RCCSDTQ), etc. methods constitute a hierarchy, which converges to the exact solution of the wave function in the given one-particle basis set.

The amplitudes t of the RCC operators are obtained by projecting bra determinants $\langle \Phi_{i_1 i_2 \dots i_k}^{a_1 a_2 \dots a_k} | e^{-\hat{T}} = \langle \Phi_0^N | a_1^+ i_1^- a_2^+ i_2^- \dots a_k^+ i_k^- e^{-\hat{T}}$ from the left of the Schrödinger equation $\hat{H}|\Psi_0\rangle = E_0|\Psi_0\rangle$, with the ground state energy E_0 , as

$$\langle \Phi_{i_1 i_2 \dots i_k}^{a_1 a_2 \dots a_k} | \bar{H} | \Phi_0 \rangle = E_0 \delta_{k,0}, \quad (k = 1, \dots, N), \quad (3)$$

where $\bar{H} = e^{-\hat{T}} \hat{H} e^{\hat{T}} = (\hat{H} e^{\hat{T}})_c$ for the subscript c means connected terms between the atomic Hamiltonian \hat{H} with the \hat{T} operators are only retained.

We have considered the Dirac-Coulomb (DC) Hamiltonian in our calculation for the free atom, which in atomic units (a.u.) is given by

$$H = \sum_{i=1}^N [c\boldsymbol{\alpha}_i \cdot \mathbf{p}_i + (\beta_i - 1)c^2 + V_n(r_i)] + \frac{1}{2} \sum_{i,j} \frac{1}{r_{ij}} \quad (4)$$

where $\boldsymbol{\alpha}$ and β are the Dirac matrices, c is the speed of light, the nuclear potential $V_n(r)$ is determined using the Fermi-charge distribution, and r_{ij} is the radial distance between the electrons located at r_i and r_j . To obtain

wave function of the endohedral confined atom, we introduce a short range spherical model potential U along with the DC Hamiltonian defining as

$$U(r) = \begin{cases} -U_0, & \text{for } r_0 \leq r \leq r_0 + \Delta \\ 0, & \text{otherwise} \end{cases} \quad (5)$$

where r_0 is the inner radius, Δ is the thickness and U_0 is the depth of the potential well.

The IP of an electron of orbital a in the atom is estimated in the RCC theory by expressing [18]

$$|\Psi_a\rangle = e^T(1 + R_a)|\Phi_a\rangle, \quad (6)$$

where the reference state is constructed as $|\Phi_a\rangle = a_a|\Phi_0\rangle$ with a_a is the corresponding annihilation operator for the electron in orbital a and R_a is another RCC operator introduced to take care of the extra correlation effects that was included through the detached electron. The IP (E_a) and amplitude solving equations for the R_a wave operators are given by

$$\langle\Phi_a^*|[(He^T) - E_a]\{1 + R_a\}|\Phi_a\rangle = \delta_{a,*} \quad (7)$$

where $|\Phi_a^*\rangle$ designates excited configuration determinants from $|\Phi_a\rangle$ for the R_a amplitude determination else it corresponds to $|\Phi_a\rangle$ to estimate IP of the electron from orbital a . This equation contains non-linear terms and also both the energy and amplitude determining equations are inter-dependent. These solutions are obtained adopting the self-consistent procedure.

The excited states ($|\Psi_K(J, \pi)\rangle$) of the Ca atom with angular momentum J and parity π is obtained by operating excitation operators Ω_K on $|\Psi_0\rangle$ as [19]

$$|\Psi_K(J, \pi)\rangle = \Omega_K(J, \pi)|\Psi_0\rangle, \quad (8)$$

where K corresponds to level of excitations. The eigenvalue (E_L) and eigenfunction for the L^{th} excited state are obtained by diagonalizing the above equation as

$$\langle\Phi_L(J, \pi)|(He^T)\Omega_K(J, \pi)|\Phi_0\rangle = E_L\langle\Phi_L(J, \pi)|\Omega_L(J, \pi)|\Phi_0\rangle. \quad (9)$$

In this expression, $|\Phi_L\rangle$ has a definite value of J and π and solutions are obtained in the iterative procedure using the Davidson's diagonalization algorithm for the non-symmetric matrix [20].

We evaluate α_0 by expressing the RCC wave function as [21]

$$|\tilde{\Psi}_0\rangle = e^{\hat{T}^{(0)} + |\tilde{\mathcal{E}}|\hat{T}^{(1)}}|\Phi_0\rangle, \quad (10)$$

where $\hat{T}^{(0)}$ represents the RCC operator that accounts for electron correlation effects due to the electromagnetic interactions only and $\hat{T}^{(1)}$ takes care of correlation effects due to both the electromagnetic interaction and the D operator, respectively, to all-orders. In the perturbative expansion, this corresponds to

$$|\Psi_0^{(0)}\rangle = e^{\hat{T}^{(0)}}|\Phi_0\rangle \quad \text{and} \quad |\Psi_0^{(1)}\rangle = e^{\hat{T}^{(0)}}\hat{T}^{(1)}|\Phi_0\rangle. \quad (11)$$

Both $|\Psi_0^{(0)}\rangle$ and $|\Psi_0^{(1)}\rangle$ can be determined by obtaining amplitudes of the $\hat{T}^{(0)}$ and $\hat{T}^{(1)}$ RCC operators. The amplitude determining equation for $\hat{T}^{(0)}$ is same as Eq. (3) for the DC Hamiltonian. The $\hat{T}^{(1)}$ amplitude determining equation is given by

$$\langle\Phi_{i_1 i_2 \dots i_k}^{a_1 a_2 \dots a_k}|\overline{H}^{DC}\hat{T}^{(1)} + \overline{D}|\Phi_0\rangle = 0. \quad (12)$$

It to be noted that for solving the amplitudes of $\hat{T}^{(0)}$, the projected $\langle\Phi_{i_1 i_2 \dots i_k}^{a_1 a_2 \dots a_k}|$ determinants have to be even parity whereas they are the odd-parity for evaluating the $\hat{T}^{(1)}$ amplitudes. We have considered the RCCSD method approximation in the RCC theory.

After obtaining these solutions, we evaluate α_0 as [6, 22]

$$\alpha_0 = 2\langle\Phi_0|e^{T^{(0)\dagger}}De^{T^{(0)}}T^{(1)}|\Phi_0\rangle_{fc}, \quad (13)$$

where fc stands for the fully-contracted terms. The above expression contains a non-terminating series $e^{T^{(0)\dagger}}De^{T^{(0)}}$. This is computed self-consistently as discussed in our earlier works [22, 23]. We also perform calculation of α_0 using the RMBPT(2) and RRPA methods adopting the procedures described in Refs. [6, 22, 24]. From the differences between the results obtained by the RRPA and RCCSD method, we can find out contributions due to the non-core-polarization correlations to all-orders.

B. Cross-section calculations

If the interaction potential $V(r)$ of the projectile electron with the target is approximated to be spherically symmetric then the method of partial wave expansion can be employed and the entire scattering process can be described by the direct and spin-flip scattering amplitudes as

$$f(k, \theta) = \frac{1}{2ik} \sum_{l=0}^{\infty} \left((l+1)(e^{2i\delta^+} - 1) + l(e^{2i\delta^-} - 1) \right) P_l(\cos \theta) \quad (14)$$

and

$$g(k, \theta) = \frac{1}{2ik} \sum_{l=0}^{\infty} \left(e^{2i\delta^-} - e^{2i\delta^+} \right) P_l^1(\cos \theta), \quad (15)$$

respectively. Here k is the relativistic wave number, δ^\pm are the scattering phase shifts with $+$ ($-$) sign refers to up (down) spin of the projectile electron, θ is the scattering angle, and $P_l(\cos \theta)$ and $P_l^1(\cos \theta)$ are the Legendre polynomials and associated Legendre functions, respectively. The phase shifts are calculated by solving the Dirac radial equation in the field of $V(r)$ and analyzing the large- r behavior of the Dirac spherical waves.

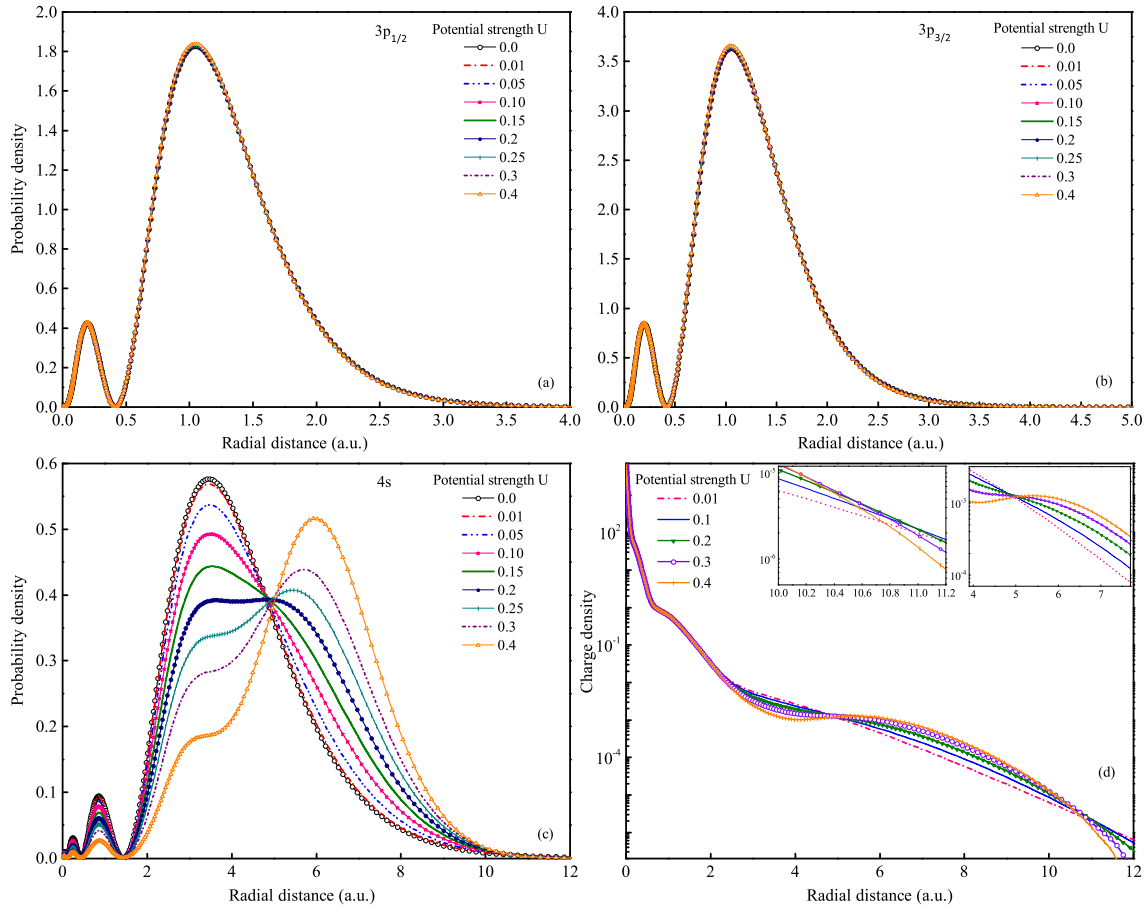


FIG. 1: (Color online) Probability densities of the $3p_{1/2}$, $3p_{3/2}$ and $4s$ orbitals are shown in (a), (b) and (c), respectively, and (d) shows charge density ($\rho(r)$) as function of the radial distance (r) and the confining potential U (in a.u.). The insets in (d) magnify the crossing of curves around 5 a.u. and large radial distances.

The DCS per unit solid angle for spin unpolarized electrons are calculated by

$$\frac{d\sigma}{d\Omega} = |f(k, \theta)|^2 + |g(k, \theta)|^2. \quad (16)$$

We obtain the ICS by integrating the DCS over the solid angle. For the computational simplicity, we express the interaction potential as $V(r) = V_{st}(r) + V_{ex}(r) - \iota V_{ab}(r)$, where V_{st} , $V_{ex}(r)$ and V_{ab} are known as the static, exchange and absorption potentials, respectively. The static potential at a general point r is evaluated using the following expression

$$V_{st}(r) = -\frac{Z}{r} - \left(\int_0^r \rho(r') 4\pi r'^2 dr' + \int_r^\infty \rho(r') 4\pi r' dr' \right) \quad (17)$$

Here Z is the nuclear charge of the atom and $\rho(r)$ is the charge densities of the confined Ca atom. We determine $\rho(r)$ first in the mean-field procedure using the DF method and then, we take into account the electron screening effects through the RCC method by including the electron correlation effects. After evaluating $V_{st}(r)$, the exchange potential is calculated using the charge density and energy dependent form suggested by Furness and

McCarthy [25]. In the elastic scattering process, there is still finite probability of occurrence of inelastic processes which we take into account through the absorption potential $V_{ab}(r)$. We define this potential in the local density approximation (LDA) as suggested by Salvat [26].

As some of the previous studies were carried out using the DFCP method (e.g. see Refs. [15, 27, 28]), we also employ the DFCP method in our calculations to demonstrate differences between the results from this method and the RCC theory by introducing the CP potential ($V_{cp}(r)$) in the interaction potential as $V(r) = V_{st}(r) + V_{ex}(r) + V_{cp}(r) - \iota V_{ab}(r)$. Here $V_{st}(r)$ and $V_{ex}(r)$ are determined using $\rho(r)$ from the DF method. This approximation for $V(r)$ may suit better for slow incident electrons as they can polarize the charge cloud of atom more causing interaction of the induced dipole moment of the atom with the projectile electron. The CP potential can be divided into two parts as short-range (V_{sr}) and long range (V_{lr}) as discussed by Salvat [26]. Here, we define $V_{sr}(r)$ in LDA [29] considering the parameters given by Pedrew and Zunger [30]. Buckingham potential [31] is employed to describe $V_{lr}(r)$ which depends upon the static dipole polarizability α_0 . It is evident now that to

define interaction potential $V(r)$ reliably it is necessary to obtain $\rho(r)$, α_0 and also excitation energies (which are required to determine $V_{ab}(r)$) as accurately as possible. Moreover, their dependencies on the well depth of the endohedral confinement need to be investigated precisely in order to study elastic scattering from the confined atom.

III. RESULTS AND DISCUSSION

A. Atomic properties

In the present work, we model the endohedral confinement potential in Eq. (5) by using the values of r_0 and Δ to be 5.8 a.u. and 1.89 a.u., respectively, as suggested by Xu et al [32]. As mentioned earlier, Hasoğlu *et al.* [3] had investigated spectroscopic properties of the confined Ca atom using the MCHF method. Here, we intend to show the differences in some of the results due to our relativistic methods compared to the MCHF calculations. We use Gaussian type orbitals (GTOs) in the DF method to obtain the single particle orbital wave functions and energies. The k^{th} GTO in an atomic orbital expansion is defined as

$$f_k(r) = e^{-\eta_k r^2}, \quad (18)$$

where η_k is an arbitrary parameter chosen suitably to produce the orbitals accurately. Using the even tempering condition as $\eta_k = \eta_0 \zeta^k$, we consider $\eta_0 = 0.00715$ and $\zeta = 1.92$ to define GTOs in our calculations. From these calculations, we observe that increasing the potential depth does not affect much the inner shell orbitals wave functions. However, for outer shell $4s$ the effect of change in the value of U is quite significant; more pronounced in the vicinity of the radial distances $r_0 - \Delta$ and $r_0 + \Delta$. To demonstrate this, we have plotted variation of probability densities of the inner $3p_{1/2}$ and $3p_{3/2}$ and outer $4s$ shells in Figs. 1(a)-(c), respectively, from the DF method. As seen, the peak of the probability density curve shifts for the $4s$ orbital towards larger r as the well deepens. All the curves cross one another nearly at inner radius r_0 of the potential well. Our results are in very good agreement with the numerical calculations by Kumar et. al. [4]. Figure 1(d) shows the electronic charge density $\rho(r)$ as a function of r at various depths. This shows the probability density of the $4s$ orbital, $\rho(r)$, also changes dramatically close to the inner-radius of the potential well. In the inset of Fig. 1(d), we show how all the curves cross approximately around $r = 5$ a.u.. This shows with increasing U value, $\rho(r)$ first decreases slowly up to $r = 10$ a.u. and falls off faster beyond 10 a.u.. After discussing wave functions, we show variation of the single particle orbital energies with the potential depth. In this case also we find that the trends match well with the results of Kumar et. al. [4] as quoted in Table I. This implies that we have correctly implemented the confined potential in our calculations.

TABLE I: Comparison of single particle orbital energies from our analytical calculations using GTOs (given as I) and numerical values reported by Kumar et al [4] (given as II) for different confined potential strength U (in a.u.).

U	4s		3p _{1/2}		3p _{3/2}		3s	
	I	II	I	II	I	II	I	II
0.000	5.34	5.34	36.71	36.71	36.28	36.29	61.55	61.55
0.005	5.37	5.37	36.75	36.75	36.33	36.34	61.59	61.59
0.010	5.40	5.40	36.79	36.79	36.37	36.37	61.63	61.63
0.050	5.65	5.65	37.14	37.14	36.72	36.72	61.97	61.97
0.090	5.93	5.93	37.54	37.53	37.12	37.10	62.36	64.35
0.130	6.24	6.24	38.00	37.95	37.59	37.53	62.82	62.77
0.140	6.35	6.33	38.09	38.06	37.67	37.64	62.90	62.88
0.170	6.62	6.60	38.45	38.41	38.03	37.99	63.26	63.22
0.200	6.91	6.88	38.65	38.77	38.44	38.35	63.67	63.57
0.200	7.02	6.98	38.99	38.89	38.58	38.47	63.80	63.69
0.220	7.13	7.09	39.13	38.01	38.71	38.59	63.93	63.81
0.250	7.47	7.41	39.54	39.39	39.12	38.96	64.33	64.18
0.290	7.96	7.87	40.10	39.88	39.64	39.46	64.90	64.66
0.310	8.23	8.11	40.34	40.12	39.92	39.70	65.12	64.90
0.330	8.50	8.36	40.60	40.35	40.20	39.93	65.40	65.13

After testing single particle orbital energies and wave functions from our DF method, we now compare the electron self-consistent field (SCF) and correlation energies with the MCHF calculations in Table II. We find our SCF energy of the free Ca atom is about 3 a.u. larger than the SCF energy reported using the MCHF method in Ref. [5]. We also perform numerical calculation of the SCF energy using the GRASP2K package [33] to validate our result. There is a good agreement between both the calculations in the relativistic approach. This justifies that the difference between the SCF energies from our calculations and the MCHF results of Hasoğlu *et al.* [5] is due to the relativistic effects. Again, the correlation energies obtained using the RMBPT(2) and RCCSD methods for both the isolated and confined Ca atoms are found to be considerably different than the values given by the MCHF method. It suggests that the relativistic and correlation corrections are inefficiently included in the MCHF method. We also find that the correlation energies from the RMBPT(2) and RCCSD methods are very close to each other and they are decreasing with the increasing value of the potential depth.

We now show the trends of IP of the confined Ca atom with well depth in Table III from the DF, RMBPT(2) and RCCSD methods. We have also given its value for the free atom and compared with the experimental value [34] in the same table. The RMBPT(2) result seems closer to the RCCSD result. We anticipate that inclusion of triple excitations in the RCC theory will improve the RCCSD result, but inclusion of these excitations demands for large computational resources. Furthermore, carrying out calculations including triple excitations for a range of well depths are too time taking. Thus, we show trends of the IP only using the RCCSD method approximation in the RCC theory framework.

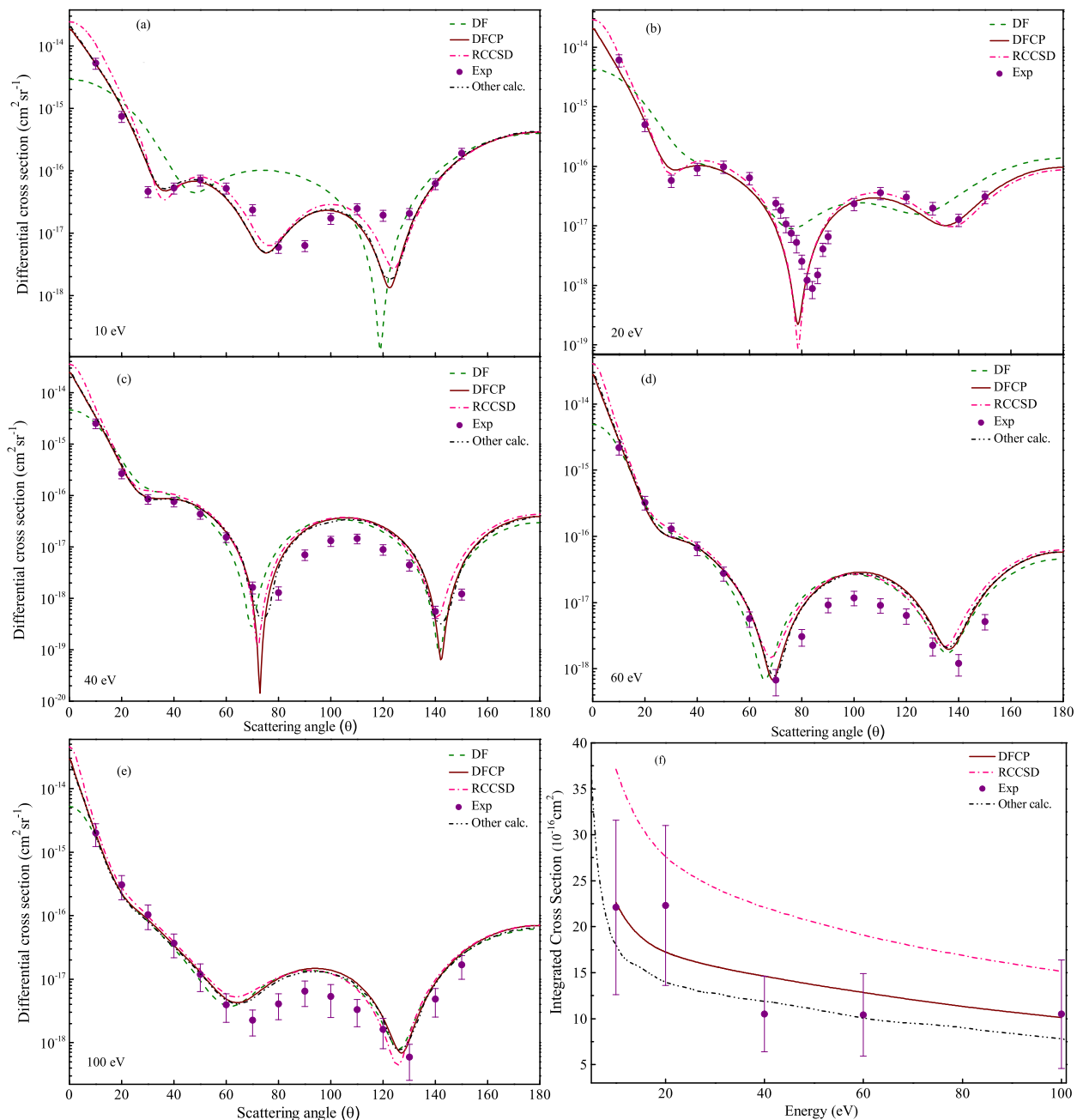


FIG. 2: (Color online) Comparison of our DCSs and ICSs from the DF, DFCP and RCCSD methods with the experimental value [14] and other available calculation [15] for the elastic scattering of an electron from an isolated Ca atom.

Determining α_0 value of an atomic system accurately in the *ab initio* approach is very challenging. We have carried out calculations of α_0 values for a variety of atomic systems precisely using our perturbative RCC method [6, 22, 24]. In our investigations, we had found RRPA can give α_0 values of atomic systems with inert gas configurations very close to the calculations using the RCCSD method and experimental values [35]. However, RRPA overestimates the α_0 values in other atomic systems while the RCCSD method is able to give very accurate results [24, 35]. From the computational point of view, RRPA takes much less time than the RCCSD

method to carry out these calculations. Since experimental value of α_0 of free Ca atom is not available precisely, we perform calculation of this quantity using the DF, RMBPT(2), RRPA and RCCSD methods. These values are given in Table IV along with the experimental result. It shows the DF method gives a lower value of α_0 in the free Ca atom, while its result increases gradually in the RMBPT(2) method and RRPA. However, the RCCSD method gives an intermediate value between the RMBPT(2) and RRPA calculations implying that there are strong cancellations between the core-polarization and other correlation effects in the RCCSD method. Our

TABLE II: Demonstration of trends of SCF and correlation energies (absolute values) as function of U . We also compare our SCF energy for the free Ca atom from the non-relativistic calculation reported by Hasoğlu et al [5] and using GRAS2K code [33]. Similarly, magnitudes of the correlation energies are also compared between the calculations using the RMBPT(2), RCCSD and MCHF methods. All the quantities are given in a.u.

U	SCF Energy		Correlation Energy		
	This work	Others	RMBPT(2)	RCCSD	MCHF [5]
0.00	679.71	676.76 [5] 679.71 [33]	0.7302	0.7487	0.223
0.01	676.79		0.7297	0.7483	0.222
0.05	679.72		0.7276	0.7465	0.221
0.10	679.74		0.7247	0.7442	0.219
0.15	679.76		0.7218	0.7419	0.217
0.20	679.79		0.7189	0.7399	0.215
0.25	679.82		0.7162	0.7379	0.213
0.30	679.85		0.7138	0.7369	0.212
0.35	679.89		0.7119	0.7379	0.211
0.40	679.93		0.7107	0.7410	0.210

TABLE III: Trends of ionization potential (IP) in cm^{-1} from the DF, RMBPT(2) and RCCSD methods as function of U (in a.u.). We also compare our results for the free Ca atom with the experimental value.

U	DF	RMBPT(2)	RCCSD	Experiment [34]
0.00	43085.69	49769.48	50138.51	49305.95
0.01	43544.77	50157.94	50520.24	
0.05	45528.67	51864.55	52180.95	
0.10	48356.92	54371.71	54654.27	
0.15	51588.43	57330.23	57645.79	
0.20	55227.19	60759.73	61198.35	
0.25	59264.59	64659.86	65301.45	
0.30	63682.83	69015.21	70031.23	
0.35	68458.74	73801.28	75508.26	
0.40	73566.84	78987.77	81725.72	

RCCSD result is also within the error bar of the experimental value [16]. We find similar trends in the α_0 values from the DF, RMBPT(2), RRPAs and RCCSD methods for finite value of the potential depth of the confined Ca atom. We also see the α_0 value of the confined Ca atom increases rapidly with increasing value of the potential depth and the perturbed amplitudes in the RCC method do not converge for relatively large magnitudes of the potential depth. In order to estimate this quantity accurately for large U values, one can extrapolate our RCCSD results from the trends of the RMBPT(2) and RRPAs calculations.

B. Elastic Scattering Cross-sections

In this sub-section, we would like to demonstrate the effects of endohedral confinement of Ca on the electron

elastic scattering cross-section. In order to assess the accuracy of our atomic structure calculations, we have calculated first DCSs for the electron and free Ca atom elastic scattering at the incident electron energies of 10, 20, 40, 60 and 100 eV and compare these calculations with the measurements reported by Milisavljević et al [14] as well as those obtained using the optical model potential approach by Hasan et al [15]. As mentioned in Sec. II B, we perform calculations using the charge densities from the DF and RCCSD methods.

In Fig. 2, we plot our DCS results for the isolated Ca atom along with the other reported values in Refs. [14] and [15]. Calculations of Hasan et al [15] are equivalent to our DFCP results and therefore, the two sets of results overlap on each other. At 10 eV, the RCCSD results explain the measurements better in comparison to the DFCP calculations in the scattering angle range $70^\circ - 110^\circ$. Also, the RCC results agree better with experimental data at 20 eV as well in the range $110^\circ - 130^\circ$. This indicates that the wave functions obtained using the RCCSD method give more reliable results at lower energies. At 20 eV, the DCS results are not reported by Hasan et al [15] and hence, they are not shown in Fig. 2(b). In general, our RCC and DFCP results are in good agreement with the measurements up to 70° electron scattering angle. Between $70^\circ - 120^\circ$ our results are slightly deviated in magnitude but agree in shape with the experimental values [14]. Beyond 120° our all the DCS, except at 60 eV, lie within the experimental error bars. Further, as expected the correlation effects play important role in the forward scattering region and at low projectile electron energy. Therefore, as the energy increases the difference between the DF and DFCP calculations diminish. We also observed that the RCC results are slightly higher in the forward scattering range. This can be due to slightly higher value of α_0 obtained by the RCCSD method in comparison to the DF method. In Fig. 2(f), we have compared ICSs from our calculations and the experimental values. The DFCP results are in better agreement with the experimental data while cross-sections from the RCCSD method are

TABLE IV: Correlation trends of dipole polarizability of the free and confined Ca atoms using the DF, RMBPT(2), RRPAs and RCCSD methods. Results are given in a.u.

U	Experiment [16]	DF	RMBPT(2)	RRPA	RCCSD
0.00	169 ± 17	122.89	151.73	182.80	157.03
0.01		125.82	155.72	187.60	161.12
0.05		138.81	173.28	208.52	180.29
0.10		158.06	198.98	238.60	209.61
0.15		180.85	228.86	272.71	245.47
0.20		207.13	262.56	310.07	288.69
0.25		236.54	299.30	349.55	Diverge
0.30		268.38	337.94	389.80	Diverge
0.35		301.61	377.09	429.48	Diverge
0.40		335.01	415.3	467.49	Diverge

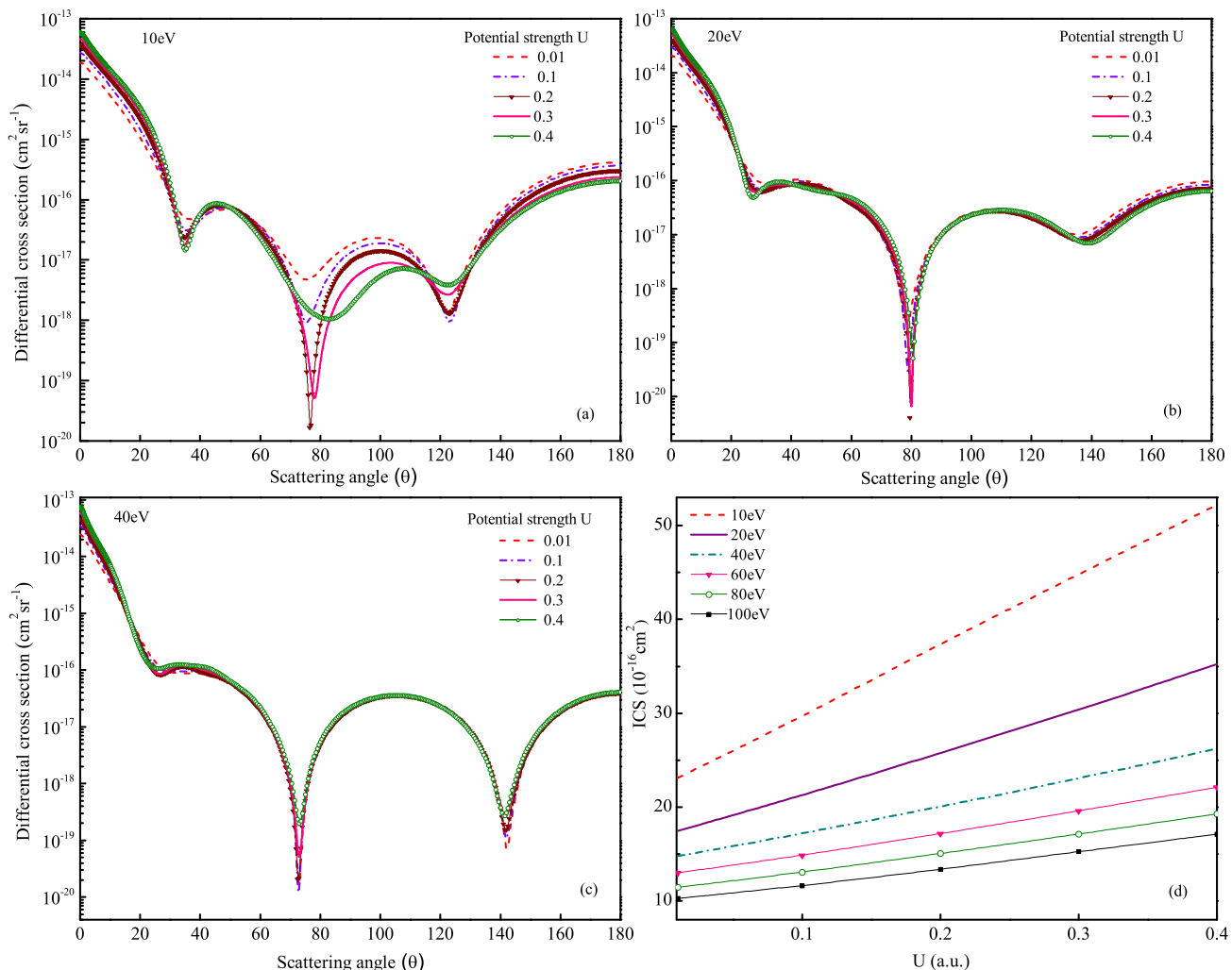


FIG. 3: (Color online) Demonstration of DCSs and ICSs using the DFCP method for the elastic scattering of an electron from a confined Ca atom as function of confining potential (U).

slightly higher than the values obtained using the DFCP method. This is again due to higher values of DCSs from the RCCSD method at small angles. Agreement of the DFCP results with the experimental values could be coincidental, but we anticipate that inclusion of contributions from the higher level excitations in our RCC theory could improve the RCCSD results. Nevertheless, we find an overall agreement of the present calculations for electron and free Ca atom elastic scattering with the previous experimental [14] and other theoretical calculations [15].

Figure 3 displays behavior of DCS as a function of confining potential U in the electron energy range 10-100 eV. Although we have performed DCS calculations using the DF, DFCP and RCCSD methods, we present here only the DFCP calculations. We have used our calculated α_0 values of the confined Ca atom to obtain polarization potentials at different U . It can be seen from the figure that the magnitude of DCS increases with increasing potential depth in the forward scattering direction. This reflects

the fact that dipole polarizability of the target Ca atom increases with increasing well depth. Also, this could be due to rise in the charge density, as shown in Fig. 1, on increasing depth of the confining potential. The shape of the DCS curves at various values of U differ significantly at low incident electron energy. This difference diminishes with the increasing energy of the projectile electron. At 10 eV the first two dips near 35° and 80° become more pronounced and deeper with increasing U . In Fig-3 (d), the ICS are shown as function of well depth at various incident electron energy. As can be seen from the figure, there is a consistent increase in the cross-sections with increasing attractive potential. At low electron energy, the rise in ICS is more with increasing value of U and the cross-section increases by 131% at 10 eV energy for a change in the value of U from 0.01 to 0.4 a.u.. However, this rise in ICS becomes slower for projectile electrons with more energy and for 100 eV ICS increases by 69% only. Thus, the slope of these cross-section curves de-

creases with increasing electron energy. It shows that the influence of the presence of the endohedral environment on the cross-section is more significant for slower projectile.

IV. CONCLUSIONS

We have carried out a detailed study of atomic structure and dynamics of endohedral confinement of Ca atom in C_{60} cage using relativistic many-body methods. Since no experimental data is available for atomic properties of the above encapsulated atom, we have evaluated self-consistent energy, correlation energy, ionization potential and dipole polarizability of this atom at different levels of approximations in the many-body methods. We found that deepening of the attractive potential well results into more tightening of the electrons to the nucleus and hence, increase in the ionization potentials. We also compared our single particle orbital energies for different values of potential depth with the corresponding results reported using numerical calculations and found very good agreement between them. Our ionization potential and dipole polarizability results for the free Ca atom agree well with the measurements. We also compared our self-consistent and correlation energies with the reported non-relativistic calculations and observe that the relativistic effects influence these results significantly.

The behavior of probability density and electronic charge density at various potential depths of the confined Ca atom obtained using the mean-field calculations are analyzed and it shows that these quantities show spectacular changes with strengthening of the confining potential. We found the probability density of the valence $4s$ shell spreads over to a broader radial distance with

increase in U in contrast to the inner shells for which it remains unaffected in the presence of the potential well. Utilizing the electronic charge densities calculated by the Dirac-Fock method and relativistic coupled-cluster theory, the differential and integrated cross-sections of elastic scattering of an electron from the free and confined Ca atoms in the incident electron energy range from 10 to 100 eV are investigated. We found our results using the core-polarization potential with the Dirac-Fock wave function and wave functions from the relativistic coupled-cluster theory are in good agreement with the measurements and previous calculations for the free Ca atom. The differential cross-sections are found to be slightly better in the relativistic coupled-cluster theory at the incident electron energies 10 and 20 eV. This shows the effectiveness of the all-order perturbative coupled-cluster theory in the low energy regime. It also emphasizes the crucial role played by the many-body methods for accurate determination of the atomic wave functions in explaining the experimental data. Further, variations in the differential and integrated cross-sections with increasing potential strength are shown. It shows differential cross-sections change dramatically; particularly at low projectile energies.

Acknowledgement

SB is thankful to the Ministry of Human Resources and Development (MHRD), Govt. of India for fellowship. RS and LS are grateful to the SERB-DST and CSIR, New Delhi, Govt. of India for the supporting research grants. B. K. S. acknowledges use of Vikram-100 HPC cluster of Physical Research Laboratory (PRL), Ahmedabad, India for the computations.

-
- [1] W. Jaskólski, Phys. Rep. **27** 1 (1996).
 [2] B. I. Dunlap, J. L. Ballester and P. P. Schmidt, J Phys. Chem. **96** 9781 (1992).
 [3] M. F. Hasoğlu, H.-L. Zhou, T. W. Gorczyca and S. T. Manson, Phys. Rev. A **87** 013409 (2013).
 [4] A. Kumar, H. R. Varma, G. B. Pradhan, P. C. Deshmukh and S. T. Manson, J. Phys. B **47** 185003 (2014).
 [5] M. F. Hasoğlu, H.-L. Zhou and S. T. Manson, Phys. Rev. A **93** 022512 (2016).
 [6] Y. Singh, B. K. Sahoo and B. P. Das, Phys. Rev. A **88**, 062504 (2013).
 [7] A. Szabo and N. Ostuland, *Modern Quantum Chemistry*, Dover Publications, Inc., Mineola, New York, First edition (revised), 1996.
 [8] I. Shavitt and R. J. Bartlett, *Many-body methods in Chemistry and Physics*, Cambridge University Press, Cambridge, UK (2009).
 [9] R. Bishop, J. Arponen and P. Pajane, *Aspects of Many-body Effects in Molecules and Extended Systems*, Berlin: Springer-Verlag (1989).
 [10] V. K. Dolmatov, M. Ya. Amusia, and L. V. Chernysheva, Phys. Rev. A **95** 012709 (2017).
 [11] V. K. Dolmatov, M. Ya. Amusia, and L. V. Chernysheva, Phys. Rev. A **92** 042709 (2015).
 [12] M. van Faassen, A. Wasserman, E. Engel, F. Zhang, and K. Burke, Phys. Rev. Lett. **99**, 043005 (2007).
 [13] M. van Faassen, J. Chem. Phys. **131**, 104108 (2009).
 [14] S. Milisavljević, D. Šević, R.K. Chauhan, V. Pejčev, D.M. Filipović, R. Srivastava, and B.P. Marinković. J. Phys. B. **38** 2371 (2005).
 [15] M. Hasan, M. A. Uddin, M. I. Hossain, A.K.F. Haque, and A.K. Basak, Can. J. Phys. **92** 206 (2014).
 [16] T. M. Miller, and B. Bederson, Phys. Rev. A **14**, 1572 (1976).
 [17] J. Cizek, Adv. Chem. Phys. **14**, 35 (1969).
 [18] D. K. Nandy and B. K. Sahoo, Phys. Rev. A **88**, 052512 (2013).
 [19] D. K. Nandy, Y. Singh and B. K. Sahoo, Phys. Rev. A **89**, 062509 (2014).
 [20] K. Hirao and H. Nakatsuji, J. Comp. Phys. **45**, 246 (1982).
 [21] B. K. Sahoo and B. P. Das, Phys. Rev. A **77**, 062516

- (2008).
- [22] Y. Singh and B. K. Sahoo, Phys. Rev. A **91**, 030501(R) (2015).
- [23] B. K. Sahoo, D. K. Nandy, B. P. Das and Y. Sakemi, Phys Rev A **91**, 042507 (2015).
- [24] Y. Singh and B. K. Sahoo, Phys. Rev. A **90**, 022511 (2014).
- [25] J.B. Furness and I.E. McCarthy. J. Phys. B **6** 2280 (1973).
- [26] F. Salvat. Phys. Rev. A **68** 012708 (2003).
- [27] S. D. Tošić, M. S. Rabasović, D. Šević, V. Pejčev, D.M. Filipović, Lalita Sharma, A. N. Tripathi, Rajesh Srivastava, and B. P. Marinković, Phys. Rev. A **77** 012725 (2008).
- [28] R. K. Gangwar, A. N. Tripathi, L. Sharma and R. Srivastava, J. Phys. B **43** 085205 (2010).
- [29] J. K. OConnell and N. F. Lane, Phys. Rev. A **27** 1893 (1983).
- [30] J.P. Perdew and A. Zunger, Phys. Rev. B **23** 5048 (1981).
- [31] R. A. Buckingham, Proceedings of the Royal Society A **168**, 264 (1938).
- [32] Y. B. Xu, M. Q. Tan, and U. Becker, Phys. Rev. Lett. **76**, 3538 (1996).
- [33] P. Jönsson, X. He, C. Froese Fischer, I.P. Grant, Comp. Phys. Comm. **177**, 597 (2007).
- [34] J. Sugar and C. Corliss, J. Phys. Chem. Ref. Data **14**, Suppl. 2 (1985).
- [35] B. K. Sahoo and B. P. Das, J. Phys.: Conf. Series **1041**, 012014 (2018).